RESEARCH

Electrical behavior of graphene under temperature effect and survey of *I–T* curve

M. Haditale[1] · R. S. Dariani[2] · E. Ghasemian Lemraski[3]

Abstract

Graphene flakes were made from electrochemical exfoliation. To study graphene planes, different volumes of graphene solutions (1, 2, 4, and 7 ml) were sprayed on glass lamellae to get different graphene planes. *I–V* curve of all samples shows ohmic behavior with resistance in the order of kΩ which increases the slope of the *I–V* curve with increasing graphene planes (spray volume). The effect of temperature on all samples shows a clear jump in *I–T* curves. It is found that up to 150 °C current is almost constant, but after that current increases highly in the range of 1.8–10 times and resistance reduces sharply. Also, samples with lower graphene planes affected highly with temperature effect.

Keywords Graphene · *I–V* curve · Jump · *I–T* curve · Resistance

Introduction

In recent years, many materials and structures were used for the fabrication of electronic devices; one of them is graphene which was discovered by Geim and Novoselov [1]. Graphene is one of the carbon allotropes with two-dimensional structure. Carbon atoms have a hexagonal structure in a plane [2]. Each carbon atom has four bonds that three of them are σ bonds in the plane and one of them is π bond which is out of the plane. The length of σ bonds is about 1.42 Å [2]. Graphene due to its particular properties, such as electrical, mechanical, optical, a unique energy band structure, and high electron mobility, is a suitable candidate for next electronic device generation like micro-supercapacitors, transistors, graphene-based sensors, biosensors, etc. [1–4]. One of the great problems for researchers is the fabrication of graphene with high quality. Since graphene exploration,

many methods were presented for the fabrication of graphene [5]. Graphene was first produced by sticky tape and then by chemical vapor deposition [6, 7] that in this method graphene was produced by using high-temperature furnace. Hummer's method is a common method for the production of graphene [8, 9]. Recently, electrochemical exfoliation of graphite has attracted attention because of its easy, fast, and environmentally friendly nature to fabricate high-quality graphene [10, 11]. Several important applications of graphene have been investigated so far such as supercapacitors [12, 13], field-effect transistors [11], thermal sensors [14], optical detectors [15], solar cells [16–18], and micro- or nanoscale photoelectric devices that were made by graphene-based hybrid nanomaterials [19]. Also in another research, the porous graphene was used to generate the gas sensor [20]. One of the best applications of graphene is in the electromagnetic field. In this field, the researchers try to design the microstructure of polymer nanocomposites to improve the electromagnetic interference shielding performances [21–24].

In this research, graphene was produced by electrochemical exfoliation because the graphene produced by this method has high quality. Then samples were sprayed on the substrate to study its electrical and structural properties. *I–V* curves of all samples show ohmic behavior, and also the slope of the *I–V* curve increases with increasing graphene planes. Then, the effect of temperature on all samples was investigated. We have seen a sharp increase

✉ M. Haditale
  Maryam.haditale@gmail.com

  E. Ghasemian Lemraski
  e.ghasemian@ilam.ac.ir

1 Department of Physics, University of Kurdistan, Sanandaj, Iran

2 Department of Physics, Alzahra University, Tehran, Iran

3 Department of Chemistry, Faculty of science, Ilam University, Ilam, Iran

at the *I–T* curve for all samples at a special temperature (150 °C). In this result, the sharp increase that has been observed for graphene in *I–T* curve is reported to the first time and it was not reported in any research yet. Also, we have seen the slope increase of *I–V* curves and more current passes through for all samples and conductivity of graphene samples increases after temperature effect.

Experimental details

Electrochemical exfoliation of graphite was performed in a two-electrode system using platinum as the counter electrode and a graphite flake as the working electrode. The distance between electrodes that were kept constant throughout the process was 1.5 cm. Different types of aqueous inorganic salt electrolyte solutions were examined and among them $(NH_4)SO_4$ exhibited the best exfoliation efficiency. Electrolyte solutions were prepared by $(NH_4)SO_4$ in water (concentration of 0.1 M and pH 7). When a direct current (DC) voltage of + 10 V was applied to a graphite electrode, the graphite flake began to dissociate and disperse into the electrolyte solution. Afterword, the exfoliated product was collected by filtration. The collected powder was then dispersed in dimethylformamide (DMF) by sonication for 10 min. Each time 250 mg of powder was dispersed in 20 ml of DMF with different sonication powers which are presented in Table 1. Samples A and B were dispersed at 20 W and 30 W, respectively. Sample C was dispersed at 20 W and centrifuged simultaneously.

To deposit the material, a spray pyrolysis system was used. To spray the sample, the air pump was used with the external pressure of 20 psi and a spray velocity of 0.01 ml/s. The diameter of nuzzling was 3 mm, and the distance between nuzzling and substrate was 11.5 cm. The substrate was glass lamellae and was placed on the heater with 100 °C during spraying. The morphology and structure of the samples were investigated by XRD (X-ray diffraction), SEM, TEM, RAMAN, and FTIR. The sheet resistance of samples was measured with a four-point probe system using a Keithley 2700 multimeter (probe spacing: 0.6 mm).

Table 1 Different sonication powers and spray volumes

Sample	Sonication power (W)	Spray volume (ml)
A	20	1, 2, 4, 7
B	W 30	1, 2, 4
C	20 and centrifugal	1, 2, 4

## Results and discussion

Morphology and structure

Sample A with 7 ml volume was used for X-ray diffraction which has a high thickness or high graphene planes. Our result showed a preferred peak at 26.5° with d-spacing of 3.3 Å (Fig. 1). Our result is in consistency with Ref. [8] with 26.5° and Ref. [10] with 26.3°.

SEM images of our samples show thin graphene flakes. Figure 2 shows a typical SEM image with the largest flakes of about 9 μm. Our images are agreed with Ref. [10] that their largest flakes were obtained 18 μm. Also, TEM images of our samples show thin graphene flakes in dimensions 200 nm (Fig. 3).

RAMAN result of our samples is presented in Fig. 4. Device using LabRAM HR800 with a wavelength of 632.8 nm is shown in Fig. 4. The peaks are marked for graphene and the glass. Figure 4 shows differently between varied spray volumes. When we increase the volume of the spray, the peak of samples' Raman increases and becomes sharper.

I–V curve

To investigate electrical properties of samples, two probe method is applied. *I–V* curves of samples showed ohmic (linear) behavior as seen in Fig. 5 for B samples (1 ml, 2 ml, and 4 ml); the result is in agreement with Ref. [25]. The figure shows that current and voltage are in the order of μm and mV, respectively. The slope of the curve is inverse of resistance and shows resistance in the order of
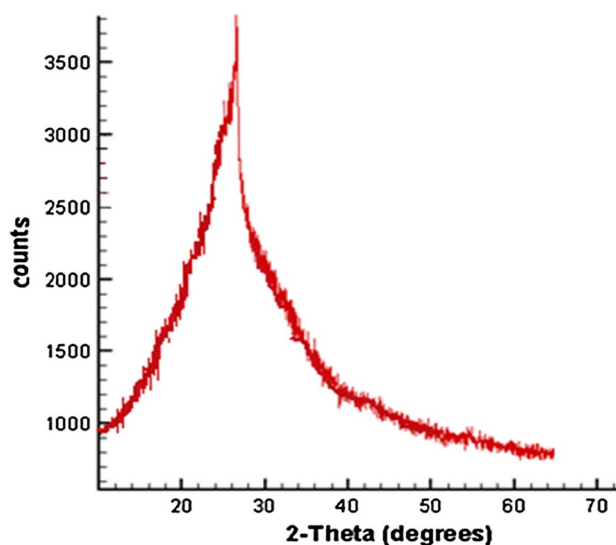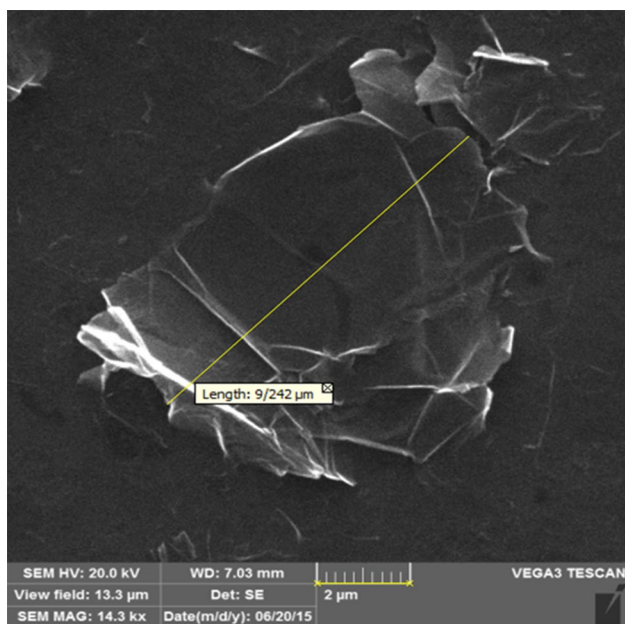

Fig. 1 XRD of sample A with 7 ml volume

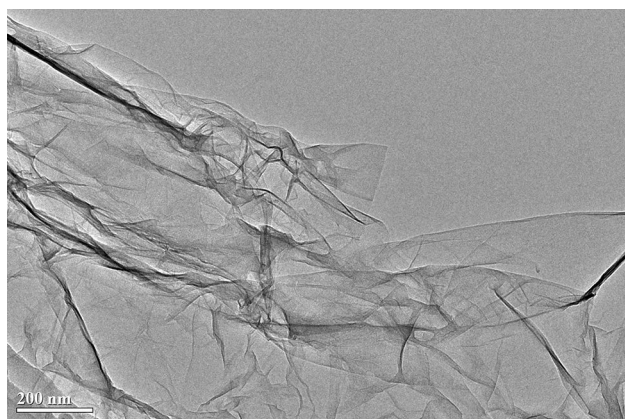**Fig. 2** SEM image of graphene flakes

Fig. 3 A TEM image of graphene flakes

kΩ. Our results are in agreement with Refs. [10, 11]. Also, our experiments show with the increasing volume of the solution, transient current increases. When we increase the volume of solution, the more flakes locate close to each other and the more contact between flakes took place. Therefore, the transient current becomes higher and resistance becomes lower.

Table 2 presents the inverse of the *I–V* curve slope which is resistance for all samples. With the increasing curve slope, the resistance of samples reduces. The sample 1 ml (C) due to centrifuge becomes dilute, so there is no connection between planes and no pass current. However, in Table 2, an increasing procedure is seen for resistance value. For similar spray volumes, resistance increases in samples B, A, and C,
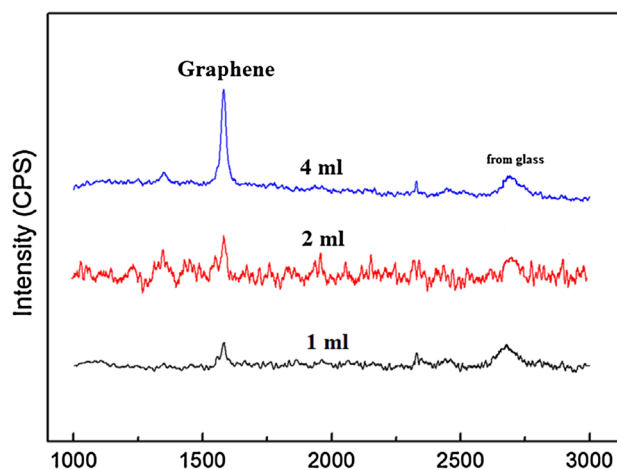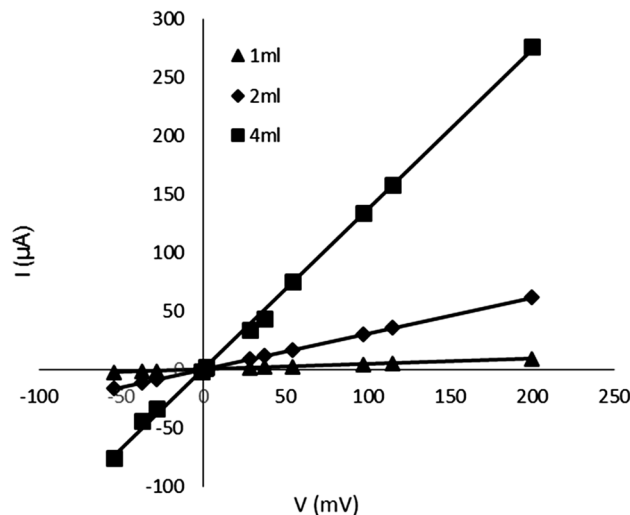

Fig. 4 RAMAN results of our samples

Fig. 5 *I–V* curves for B samples (1 ml, 2 ml, and 4 ml)

Table 2 The resistance of samples before the temperature effect

Sample	Spray volume (ml)	$R = \Delta V/\Delta I$ (kΩ)
A	1, 2, 4, 7	60.24, 3.77, 2.34, 2.76
B	1, 2, 4	21.5, 3.16, 0.72
C	1, 2, 4	∞, 1000, 5.95

respectively. These results show the last stage of fabrication effects on the electrical properties of graphene samples.

I–V curve of samples after temperature effect

After the temperature effect on samples, again their *I–V* were measured by two probs. Again all curves were obtained ohmic behavior. The order of current, voltage and resistance

was μA, mV, and kΩ, respectively. By comparing *I–V* curves of all samples before and after temperature effect, it is seen that the slope of curves increases, i.e., transient current increases. In Table 3, the resistance of all samples is presented and can be observed that the resistance of all samples reduces. These results are in agreement with Refs. [6, 7], i.e., effect of temperature on graphene reduces its resistance. However, the resistance reduction is different for various samples. For example, the resistance reduction for the sample with the lower layer is much more than the others. With the comparison of obtained values for resistance at Tables 2 and 3, the reduction rate can be calculated. The reduction rate is varied from 1.7 to 70 times that for sample C with 4 ml the highest resistance reduction is seen.
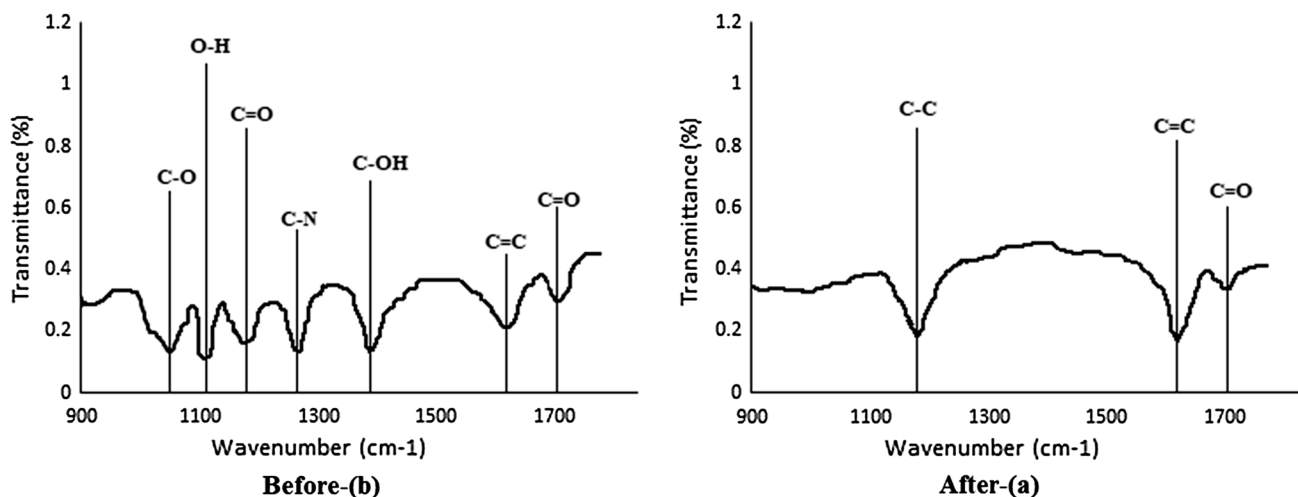
Temperature effect on samples

In this section, the temperature effect on graphene samples was studied by the *I–T* curve. For this purpose, a constant voltage of 10.5 mV was applied on samples and current variations versus temperature effects were recorded. According to Fig. 7, samples show a clear jump at 150 °C and transient current increases highly. *I–T* curves for all samples showed an obvious jump at 150 °C, and current increases strongly. We proposed two reasons for this jump. One of the reasons is the evaporation of remained DMF solution

between graphene flakes. As already mentioned, graphene is a two-dimensional plane with a honeycomb structure that each carbon atom has three strong covalent σ bonds with nearest-neighbor carbon atoms and a weak van der Waals π bond at the perpendicular direction which is ready to be bonded with other atoms. When graphene planes and DMF occur close to each other, the carbon π bond occurs with DMF (C_3H_7NO) at a perpendicular plane. By applying temperature, DMF evaporates between graphene planes, so planes condense and contact between planes gets more. Thus, transient current increases. The vapor temperature of DMF is about 154 °C, and our clear jumps are seen at 150 °C as well. To prove this hypothesis, we measured FTIR of our samples. Figure 6 shows the typical FTIR measurement of our samples before and after the temperature effect. As seen before the heating, there are seven carbon bonds in our samples: C–O stretch bond at 1060 cm^{-1}, C=O stretch bond at 1710 cm^{-1}, C–C stretch bond at 1180 cm^{-1}, C=C stretch bond at 1620 cm^{-1}, C–N stretch bond at 1250 cm^{-1}, C–OH stretch bond at 1380 cm^{-1} and O–H stretch bond at 1151 cm^{-1}, which is in agreement with Refs. [9, 26–30], and after the heating, there are three carbon bonds in our samples. C=O stretch bond at 1710 cm^{-1}, C–C stretch bond at 1180 cm^{-1} and C=C stretch bond at 1620 cm^{-1}. Then the heating breaks the van der Waals bonds and causes to vapor DMF. So the FTIR results confirm the hypothesis above.

The other reason for this jump is a percolation phenomenon. The percolation phenomenon is a mathematical concept. In physics, percolation is dealing with fluid motion from porous materials [31]. Also, the percolation threshold is a mathematical concept; below the percolation threshold, there is not any connection between consistent components. The percolation threshold is the time of components connection and exists above the percolation

**Table 3** The resistance of samples after the temperature effect

Sample	Spray volume (ml)	$R = \Delta V / \Delta I$ (kΩ)
A	1, 2, 4, 7	3.01, 1.67, 0.62, 0.95
B	1, 2, 4	1.82, 0.95, 0.43
C	1, 2, 4	∞, 14.3, 1.53

Fig. 6 FTIR result of the samples before and after temperature effect (the heating)

Table 4 Jump values and samples resistance at *I–T* curve

Sample	Spray volume (ml)	Resistance in jump (point 1) (kΩ)	Resistance in 250 °C (point 2) (kΩ)	Jump rate $(I_2 - I_1)/I_1$
A	1, 2, 4, 7	30.28, 3.53, 2.14, 2.64	3.01, 1.21, 0.7, 0.83	6.6, 2.5, 2.2, 2.1
B	1, 2, 4	11.36, 2.88, 0.68	1.63, 0.98, 0.37	4.5, 1.6, 0.9
C	2, 4	118.88, 5.4	14.86, 1.64	7.5, 2.3
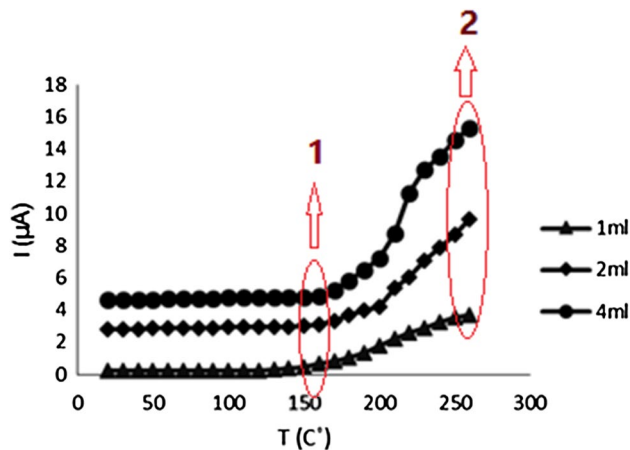
Fig. 7 *I–T* curve for sample B

threshold connection. In the case of graphene planes also can be explained by the percolation threshold phenomenon. According to the percolation threshold, graphene planes are dispersed close to each other, with temperature effect and reaching to 150 °C, graphene planes locate at connection threshold, and with increasing temperature, the connection between planes get to be more. In the *I–T* curve, when a current jump occurs, it is meant that the percolation threshold takes place. This phenomenon causes change in the current mechanism, and transient current increases. Current jump increases with decreasing thickness of samples. Samples with the lower thickness could be similar to graphene, increasing temperature causes graphene planes to become close to each other, more current passes through, and this increase occurs gradually.

To study the electrical aspect of the jump phenomenon, Table 4 presents jump value, resistance in the jump threshold (Fig. 7-arrow 1), and at 250 °C temperature (Fig. 7-arrow 2). According to Table 4, the resistance of samples at the jump threshold (1) is higher than at 250 °C temperature (2). This issue shows clearly that the effect of temperature on graphene causes a reduction in resistance. Obtained values for jump rate (Table 4) for samples with lower volume are higher and indicate that the sample with lower thickness highly affected by temperature and highest value for jump rate belongs to sample C with 2 ml volume.

Table 5 Sheet resistance before and after the temperature effect

Sample	R_s before (kΩ/sq)	R_s after (kΩ/sq)
A: 2 ml, 4 ml	0.97, 1.9	0.36, 0.39
B: 2 ml, 4 ml	2.1, 0.51	0.65, 0.32
C: 4 ml	0.48	0.12

Sheet resistance of samples before and after temperature effect

To study temperature effect on samples, the sheet resistance of samples was measured with the four-probe system. Distance between probes was 0.6 mm, and current from two external probes and voltage from two internal probes were measured. The data are presented in Table 5. Our results showed that sheet resistance reduces after temperature effect which is agreed with Refs. [6, 7].

Conclusions

In this research, fabrication of graphene by electrochemical exfoliation is used. Then, we have used spray pyrolysis for deposition graphene on the substrate. Structural characterizations of samples, such as fabrication of graphene planes, carbon existence, and carbon bonds, are confirmed by XRD, SEM, TEM, RAMAN, and FTIR. All samples showed similar electrical properties. *I–V* curve of samples indicates ohmic (linear) behavior, and resistance is obtained in the order of kΩ. With the increasing number of graphene layers, the slope of the sample curve increases, which means that resistance decreases. Temperature effect showed a slope of *I–V* increases which means that resistance decreases. *I–T* curve shows there is a clear jump in current at 150 °C, and we proposed two reasons for this jump.

References

1. Geim, A.K., Novoselov, K.S.: The rise of graphene. Nat. Mater. **6**, 183 (2007)

2. Cooper, D.R., D'Anjou, B., Ghattamaneni, N., Harack, B., Hilke, M., Horth, A., Majlis, N., Massicotte, M., Vandsburger, L., Whiteway, E., Yu, V.: Experimental review of graphene. ISRN Condens. Matter Phys. **2012**, 1–56 (2011)

3. Wu, Z.S., Parvez, K., Feng, X., Müllen, K.: Graphene-based in-plane micro-supercapacitors with high power and energy densities. Nat. Commun **4**, 2487 (2013)

4. Park, S., Ruoff, R.S.: Chemical methods for the production of graphenes. Nat. Nanotechnol. **4**, 217 (2009)

5. Novoselov, K.S., Geim, A.K., Morozov, S.V., Jiang, D., Zhang, Y., Dubonos, S.V., Grigorieva, I.V., Firsov, A.A.: Electric field effect in atomically thin carbon films. Science **306**, 666 (2004)

6. Kholmanov, I.N., Magnuson, C.W., Aliev, A.E., Li, H.F., Zhang, B., Suk, J.W., Zhang, L.L., Peng, E., Mousavi, S.H., Khanikaev, A.B., Piner, R., Shvets, G., Ruoff, R.S.: Improved electrical conductivity of graphene films integrated with metal nanowires. Nano Lett. **12**, 5679–5683 (2012)

7. Park, H.J., Meyer, J., Roth, S., Kalova, V.S.: Growth and properties of few-layer graphene prepared by chemical vapor deposition. Carbon **48**, 1088–1094 (2010)

8. Wang, G., Yang, J., Park, J., Gou, X., Wang, B., Liu, H., Yao, J.: Facile synthesis and characterization of graphene nanosheets. J. Phys. Chem. C **112**, 8192–8195 (2008)

9. Muthoosamy, K., Bai, R.G., Abubakar, I.B., Sudheer, S.M., Lim, H.N., Loh, H.S., Huang, N.M., Chia, C.H., Manickam, S.: Exceedingly biocompatible and thin-layered reduced graphene oxide nanosheets using an eco-friendly mushroom extract. Int. J. Nanomed. **10**, 1505–1519 (2015)

10. Parvez, K., Wu, Z.S., Li, R., Liu, X., Graf, R., Feng, X., Müllen, K.: Exfoliation of graphite into graphene in aqueous solutions of inorganic salt. J. Am. Soc. **136**, 6083–6091 (2014)

11. Parvez, K., Li, R., Puniredd, S.R., Hernandez, Y., Hinkel, F., Wang, S., Feng, X., Müllen, K.: Electrochemically exfoliated graphene as solution-processable, highly conductive electrodes for organic electronics. Am. Chem. Soc. **7**(4), 3598–3606 (2013)

12. Wang, H., Hao, Q., Yang, X., Lu, L., Wang, X.: Graphene oxide doped polyaniline for supercapacitors. Electrochem. Commun. **11**, 1158–1161 (2009)

13. Wu, Z.-S., Parvez, K., Winter, A., Vieker, H., Liu, X., Han, S., Turchanin, A., Feng, X., Müllen, K.: Layer-by-layer assembled heteroatom-doped graphene films with ultrahigh volumetric capacitance and rate capability for micro-supercapacitors. Adv. Mater. **26**, 4552–4558 (2014)

14. Kim, J., Oh, S.D., Kim, J.H., Shin, D.H., Kim, S., Choi, S.-H.: Graphene/Si-nanowire heterostructure molecular sensors. Sci. Rep. **4**, 5384–5388 (2014)

15. Kim, C.O., Hwang, S.W., Kim, S., Shin, D.H., Kang, S.S., Kim, J.M., Jang, C.W., Kim, J.H., Lee, K.W., Choi, S.-H., Hwang, E.: High-performance graphene-quantum-dot photodetectors. Sci. Rep. **4**, 5603–5608 (2014)

16. Li, X., Zhu, H., Wang, K., Cao, A., Wei, J., Li, C., Jia, Y., Li, Z., Li, X., Wu, D.: Graphene-on-silicon Schottky junction solar cells. Adv. Mater. **22**, 2743–2748 (2010)

17. Wang, X., Zhi, L., Mullen, K.: Transparent, conductive graphene electrodes for dye-sensitized solar cells. Nano Lett. **1**, 323–327 (2008)

18. Shi, E., Li, H., Yang, L., Zhang, L., Li, Z., Li, P., Shang, Y., Wu, S., Li, X., Wei, J., Wang, K., Zhu, H., Wu, D., Fang, Y., Cao, A.: Colloidal antireflection coating improves graphene–silicon solar cells. Nano Lett. **13**, 1776–1781 (2013)

19. Wang, J., Mu, X., Sun, M., Mu, T.: Optoelectronic properties and application of graphene-based hybrid nanomaterials and van der Waals heterostructures. Appl. Mater. Today **16**, 1–20 (2019)

20. Wang, Y., Yang, M., Liu, W., Dong, L., Chen, D., Peng, C.: Gas sensors based on assembled porous graphene multilayer frameworks for DMMP detection. J. Mater. Chem. C **7**, 1–9 (2019)

21. Liang, C., Song, P., Qiu, H., Huangfu, Y., Lu, Y., Wang, L., Kong, J., Gu, J.: Superior electromagnetic interference shielding performances of epoxy composites by introducing highly aligned reduced graphene oxide films. Compos. Part A **124**, 105512 (2019)

22. Songa, P., Lianga, C., Wanga, L., Qiua, H., Gub, H., Konga, J., Gu, J.: Obviously improved electromagnetic interference shielding performances for epoxy composites via constructing honeycomb structural reduced graphene oxide. Compos. Sci. Technol. **181**, 107698 (2019)

23. Huangfu, Y., Ruan, K., Qiu, H., Lu, Y., Liang, C., Kong, J., Gu, J.: Fabrication and investigation on the PANI/MWCNT/thermally annealed graphene aerogel/epoxy electromagnetic interference shielding nanocomposites. Compos. Part A **121**, 265–272 (2019)

24. Lianga, C., Qiua, H., Hana, Y., Guc, H., Songa, P., Wanga, L., Konga, J., Caod, D., Gua, J.: Superior electromagnetic interference shielding 3D graphene nanoplatelets/reduced graphene oxide foam/epoxy nanocomposites with high thermal conductivity. J. Mater. Chem. C **7**(9), 2725–2733 (2019)

25. Paustovsky, A.V., Sheludko, V.E., Ya, E., Telnikov, E., Marchuk, A.K., Kremenitsky, V.V., Tarasyuk, O.P., Rogalsky, S.P.: The structural and electrical properties of graphene-containing thick films. Powder Metall. Met. Ceram. **57**(5–6), 285–292 (2018)

26. Gao, R., Hu, N., Yang, Z., Zhu, Q., Chai, J., Su, Y., Zhang, L., Zhang, Y.: Paper-like graphene-Ag composite films with enhanced mechanical and electrical properties. Nanoscale Res. Lett. **8**(1), 32 (2013)

27. Pfaffeneder-Kmen, M., Casas, I.F., Naghilou, A., Trettenhahn, G., Kautek, W.: A multivariate curve resolution evaluation of an in situ ATR-FTIR spectroscopy investigation of the electrochemical reduction of graphene oxide. Electrochim. Acta **255**, 160–167 (2017)

28. Al-Gaashani, R., Najjar, A., Zakaria, Y., Mansour, S., Atieh, M.A.: XPS and structural studies of high quality graphene oxide and reduced graphene oxide prepared by different chemical oxidation methods. Ceram. Int. **45**(11), 14439–14448 (2019)

29. Tang, Z., Zhang, L., Zeng, C., Lin, T., Guo, B.: General route to graphene with liquid-like behavior by non-covalent modification. Soft Matter **8**, 9214–9220 (2012)

30. Chieng, B.W., Ibrahim, N.A., Yunus, W.M.Z.W., Hussein, M.Z.: Poly (lactic acid)/poly (ethylene glycol) polymer nanocomposites: effects of graphene nanoplatelets. Polymers **6**(1), 93–104 (2014)

31. Newman, M.E.J., Ziff, R.M.: Efficient monte carlo algorithm and high-precision results for percolation. Phys. Rev. Lett **85**, 4104–4107 (2000)